The use of Pyrimidine and Pyrazine Bridges as a Design Strategy to Improve the Performance of Thermally Activated Delayed Fluorescence Organic Light Emitting Diodes

Paloma L. dos Santos,[a]† Dongyang Chen,[b]† Pachaiyappan Rajamalli,[b] Tomas Matulaitis,[b] David B. Cordes,[b] Alexandra M. Z. Slawin,[b] Denis Jacquemin,[c] Eli Zysman-Colman[b] and Ifor D. W. Samuel*[a]*

[a] Organic Semiconductor Centre, SUPA, School of Physics and Astronomy, University of St Andrews, St Andrews, Fife KY16 9SS, United Kingdom.

[b] Organic Semiconductor Centre, EaStCHEM School of Chemistry, University of St. Andrews, St. Andrews, Fife, KY16 9ST, United Kingdom.

[c] CEISAM, UMR-CNRS 6230, University of Nantes, 2, rue de la Houssinière, 44322 Nantes, France.

†These authors contributed equally to this manuscript.

*eli.zysman-colman@st-andrews.ac.uk, idws@st-andrews.ac.uk

Keywords: TADF, organic light emitting diodes, pyrimidine, pyrazine, blue OLED, intramolecular hydrogen bond

Abstract

We present a study of two isomeric thermally activated delayed fluorescence (TADF) emitters 9,9'-(sulfonylbis(pyrimidine-5,2-diyl))bis(3,6-di-*tert*-butyl-9H-carbazole) (**pDTCz-DPmS**) and 9,9'-(sulfonylbis(pyrazine-5,2-diyl))bis(3,6-di-*tert*-butyl-9H-carbazole) (**pDTCz-DPzS**). The use of pyrimidine and pyrazine as bridging units between the electron donor and acceptor moieties is found to be advantageous compared to the phenyl- (**pDTCz-DPS**) and pyridine-based analogues (**pDTCz-3DPyS** and **pDTCz-2DPyS**). Conformational modulation of the donor groups as a function of the bridge results in high photoluminescence quantum yields (Φ_{PL} > 68%) and small energy gaps between singlet and triplet excited states (ΔE_{ST} < 160 meV). OLEDs using **pDTCz-DPmS** and **pDTCz-DPzS** as emitters exhibit blue and green electroluminescence, respectively, with higher maximum external quantum efficiencies (EQE_{max} of 14% and 18%, respectively) and reduced efficiency roll-off as compared to the reference devices using **pDTCz-DPS**, **pDTCz-3DPyS**, and **pDTCz-2DPyS** as the emitters. Our results provide a more complete understanding on the impact of the bridge structure in D-A-D TADF systems on the optoelectronic properties of the emitter, and how the balance between color purity and EQE in the devices can be controlled, advancing the design strategies for TADF emitters.

Introduction

Research into the design of thermally activated delayed fluorescence (TADF) compounds for organic light emitting diodes (OLEDs) has flourished over the past seven years, driven by the discovery that OLEDs employing purely organic emitters can realize internal quantum efficiencies (IQE) surpassing the 25% imposed by spin statistics[1] governing classic fluorophores. In organic compounds that emit via a TADF mechanism, non-emissive triplet states are upconverted to emissive singlet states via a reverse intersystem crossing (rISC) using

latent thermal energy.[2,3] In this fashion, OLEDs relying based on TADF compounds can attain 100% IQE without the requirement of using scarce noble metal phosphorescent complexes, materials presently employed as red and green emitters in commercial OLEDs.

A major challenge in OLEDs is the development of bright and stable blue devices that satisfy the strict color purity requirements that industry imposes for high-definition displays. For example, the National Television System Committee (NTSC) states blue devices should show *Commission Internationale de l'Éclairage* (CIE) coordinates of (0.14, 0.08). It is particularly challenging to generate highly emissive and stable blue OLEDs for a number of reasons, including the difficulty to inject charges into the emitter due to its wide electrochemical gap, and emitter degradation resulting from bond dissociation energies of the emitter that are on the same order as its emissive state energy.[4,5] Further, the number of suitable host materials with even larger eletrochemical gaps than that of the emitter are limited, making a viable device architecture difficult to achieve. Presently, a huge focus on TADF research has been devoted towards designing blue emitters and there exist several reports of devices showing a maximum external quantum efficiency (EQE_{max}) exceeding 20% and supressed efficiency roll-off.[6–8] However, further optimization of their molecular design and the corresponding device performance is required to improve the efficiency roll-off in order to make them attractive to industry, allowing them to replace the presently used fluorescent blue emitters in commercialized OLEDs.

When designing TADF molecules it is necessary but not sufficient that the emitters (i) possess a small energy gap between the singlet and triplet excited states (ΔE_{ST}) in order to ensure an efficient rISC process, and (ii) are structurally rigid to supress non-radiative decay pathways in order to maximize photoluminescence quantum yields (Φ_{PL}). A large number of TADF emitters are based on a highly twisted D-A-D conformation where, with suitable choices of donor (D) and acceptor (A) moieties, small ΔE_{ST} values can be achieved. These molecules emit from a singlet excited state (S_1) with strong intramolecular charge transfer character (^{1}CT), which is energetically very close to a triplet state with dissimilar symmetry (such as a locally excited triplet state, ^{3}LE).[9,10] However, reducing ΔE_{ST} through minimizing the exchange integral between the frontier orbitals also leads to a reduced oscillator strength, *f*, of the emissive S_1 state. So, there remains a design challenge where both ΔE_{ST} and *f* are optimized. The strategy employed in this study is to reduce the non-radiative decay pathways by constraining the conformational landscape available in D-A-D compounds.[11,12]

We previously reported[13] how replacement of the phenylene bridges in **pDTCz-DPS** (originally named **3**, renamed here for clarity),[14] where D is a 3,6-di-*tert*-butyl-9H-carbazole (**DTCz**), with pyridyl groups promotes a more planarized conformation between either the donor and the bridge or the two bridging aryl groups about the SO_2 moiety, while also strengthening the nature of the acceptor. This leads to an enhanced Φ_{PL} in the film with only a small red-shift in the photoluminescence spectrum, which translates into an improved

device performance while maintaining the blue color (λ_{EL}= 461 nm). Here, we extend this concept by exploring the impact of pyrimidine and pyrazine bridges in **DTCz**-sulfone containing D-A-D emitters. Two isomeric emitters, 9,9'-(sulfonylbis(pyrimidine-5,2-diyl))bis(3,6-di-*tert*-butyl-9H-carbazole) (**pDTCz-DPmS**) and 9,9'-(sulfonylbis(pyrazine-5,2-diyl))bis(3,6-di-*tert*-butyl-9H-carbazole) (**pDTCz-DPzS**) (Figure **1**). Both emitters contain more planar donor-bridge conformations that are stabilized by intramolecular hydrogen bonding. The photophysical analysis revealed that both emitters possess small ΔE_{ST} and high Φ_{PL}. We show that, with the pyrimidine bridge, blue-emitting OLEDs using **pDTCz-DPmS** are obtained with EQE_{max}= 14%, and EQE_{100} = 7% (at 100 cd/m^2), representing a modest improvement in the EQE_{max} and a substantial improvement in the efficiency roll-off compared to our previously reported devices with **pDTCz-3DPyS**.[13] With the pyrazine bridge in **pDTCz-DPzS**, a much larger enhancement in the EQE_{max} and much-reduced efficiency roll-off is obtained (EQE_{max}=18%, EQE_{100}=14%). However, due to the use of the stronger **DPzS** acceptor strength green OLEDs are obtained. Thus, with this work, a more profound understanding about the subtle relationship between molecular structure and the TADF mechanism is achieved, advancing the design strategies of TADF materials.

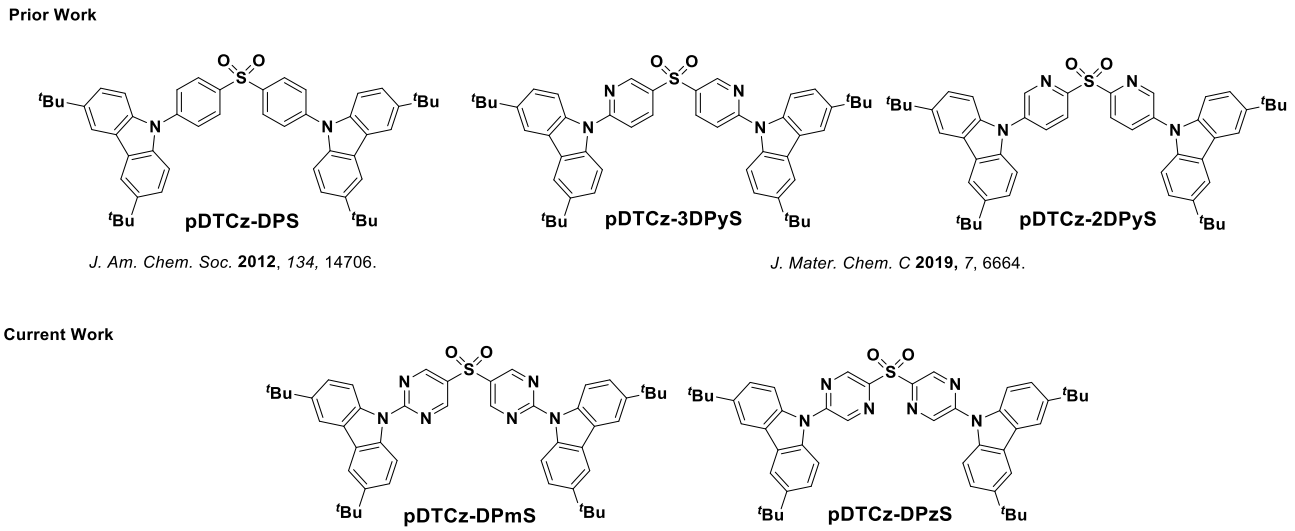

Figure **1**: Chemical structures of **pDTCz-DPmS**, **pDTCz-DPzS**, **pDTCz-3DPyS**, **pDTCz-2DPyS** and **pDTCz-DPS**.

Results and discussion

Synthesis and Chemical Characterization

The syntheses of **pDTCz-DPmS** and **pDTCz-DPzS** are outlined in Scheme **1**. The two emitters were accessed in three steps consisting of two copper-catalysed Ullmann reactions followed by oxidation of the intermediate sulfide to the sulfone. Both emitters were characterized by a combination of ^{1}H and ^{13}C NMR spectroscopy (Figures **S1-S4**), high-resolution mass spectrometry, melting point determination, and elemental analysis (Figures **S5-S6**). The two emitters were purified by silica gel chromatography and temperature gradient

vacuum sublimation, and the purity was established by high performance liquid chromatography (HPLC) analysis (Figures **S7-S8**). The structures of **pDTCz-DPzS** and **pDTCz-DPmS** were confirmed by single crystal X-ray diffraction analysis (Figure **2**). The conformation of **pDTCz-DPmS** in the crystal reveals a very small dihedral angle between the donor DTCz and adjoining pyrimidine [12.2(3)°] bridge that is coupled with an N···H distances of 2.30 and 2.35 Å between the pyrimidine nitrogen and the proximal hydrogen atoms of the *tert*-butyl carbazole, indicative of a moderate hydrogen bond. For **pDTCz-DPzS**, only the *gauche* conformer was found in the crystal structure where the two pyrazine rings are symmetrically disposed, which is similar to the conformer found in the crystal structure of **pDTCz-3DPyS**. The dihedral angle between the donor DTCz and adjoining pyrazine is larger at 38.20(8)° in the single crystal than that of **pDTCz-DPmS**, and is slightly smaller than that found in **pDTCz-2DPyS** (42.77 and 51.66°)[13] and **pDTCz-3DPyS** [41.54(6)°]. The distance between one of the two pyrazine nitrogen atoms and one of the proximal hydrogen atoms of the *tert*-butyl carbazole in **pDTCz-DPzS** is almost identical to that seen in **pDTCz-3DPyS**, 2.56 Å compared to 2.57 Å, again indicative of a weak hydrogen bond. In **pDTCz-2DPyS** no equivalent hydrogen bond is present.

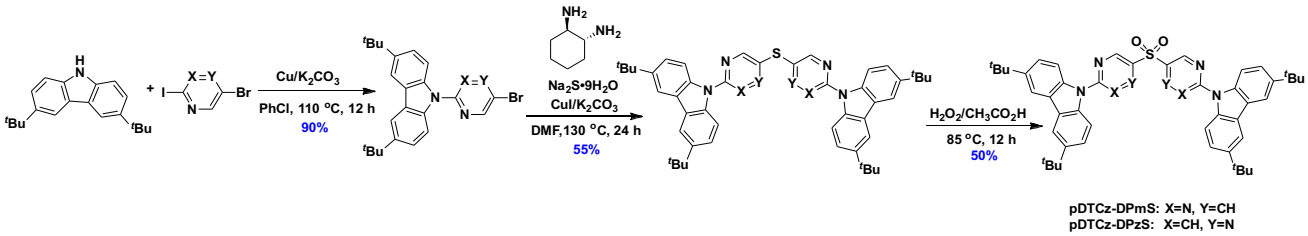

Scheme **1**. Synthesis of **pDTCz-DPzS** and **pDTCz-DPmS**

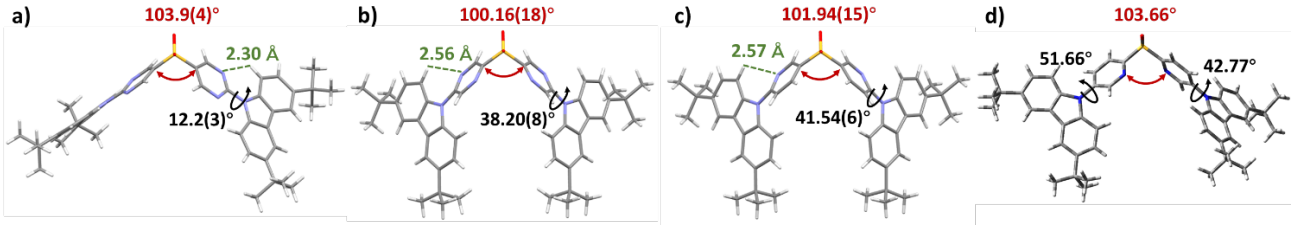

Figure **2**. Crystal structure of (a) **pDTCz-DPmS**, (b) **pDTCz-DPzS** and (c) **pDTCz-3DPyS** and (d) **pDTCz-2DPyS** (structure taken from reference [13]). Solvent molecules and minor components of disorder omitted.

Theoretical Calculations

Density Functional Theory (DFT) calculations, and more precisely PBE0/6-31G(d,p) calculations,[15,16] were performed for **pDTCz-DPzS** and **pDTCz-DPmS** to gain insights into the lowest energy conformation in the ground state, the associated energies, and the nature of the frontier molecular orbitals. Optimization of the ground state geometries started from the X-ray single crystal structures. The Tamm-Dancoff approximation (TDA)[17,18] of time-dependent density functional theory (TD-DFT) was applied to determine the nature of both the excited singlet and triplet states as well as to estimate ΔE_{ST}. In the ESI, we show that this level of theory

provides results consistent with electron-correlated wavefunction approaches in our case. For **pDTCz-DPzS**, both *anti* and *gauche* conformers were optimized, and we recall that the *gauche* conformation is found in the crystal structure (Figures **2**, **3** and **S9**). The *anti* conformer is the most stable by 7.7 kJ·mol^{-1}; the difference with the crystal structure being probably related to packing effects neglected in the calculation. We compute that the *anti* conformation of **PDTCz-DPzS** is more stable by 7.7 kJ.mol^{-1} compared to its *gauche* counterpart, and that the barrier for the *gauche* to *anti* conversion is rather small (10.4 kJ·mol^{-1}), so DFT indicates that only the latter conformation will be present in solution at room temperature. An analysis of the relative energies of the two conformers in the absence of donor groups revealed a similar interconversion barrier of 10.4 kJ·mol^{-1} (Figure **S11**). Compound **pDTCz-DPmS** has a more symmetric structure than **pDTCz-DPzS** and therefore presents only one conformer. The rotational barrier between the donor moiety and the bridge is 52 kJ·mol^{-1} in **pDTCz-DPmS** but only 23 kJ·mol^{-1} in **pDTCz-DPzS**. Both barriers are sufficiently small to permit rapid rotation of the donor about the bridge in fluid solution.

The DFT-optimized structure of **pDTCz-DPmS** reveals an almost completely planar donor-bridge conformation with the dihedral angle between the DTCz and pyrimidine bridge as small as [0.66(7)°]. The N···H distances between the pyrimidine nitrogen and the proximal hydrogen atoms of DTCz were found to be 2.24 Å, which are slightly shorter than those found in the single crystal. Turning to the *gauche* conformer of **pDTCz-DPzS**, the DFT-optimized structure predicts a dihedral angle between the DTCz and pyrazine of 32.9°, which is ca. 6° smaller than that found in the crystal structure. Analogously, the N···H distances between the pyrimidine nitrogen and the proximal hydrogen atoms were found to be shorter than those found in single crystal (2.37 Å compared to 2.56 Å and 2.57 Å, respectively). Despite these small deviations in geometry, the DFT-optimized structures generally match closely those found in the single crystal.

Owing to the relatively small dihedral angles between the donor and the bridge, the HOMO of both emitters is extended from the donor to the heterocyclic bridge, and are of very similar energy, differing by no more than 90 meV (Figure **3**). The LUMO is more strongly affected by the positions of the nitrogen atoms relative to the sulfur atom within the heterocyclic acceptor (see Figures **S11-S12** for an expanded analysis of the relative energetics of the acceptor). The LUMO of **pDTCz-DPmS** (1.86 eV) is destabilized by 250 meV than that of **pDTCz-DPzS** *gauche* form (-2.11 eV). The *anti* conformer has a higher lying LUMO than the *gauche* conformer by 180 meV. In both conformers of **pDTCz-DPzS**, the LUMO is mainly localized over the entire acceptor moiety with a minor contribution extending to the donor while in **pDTCz-DPmS** there is a delocalization of the LUMO over the entire molecule.

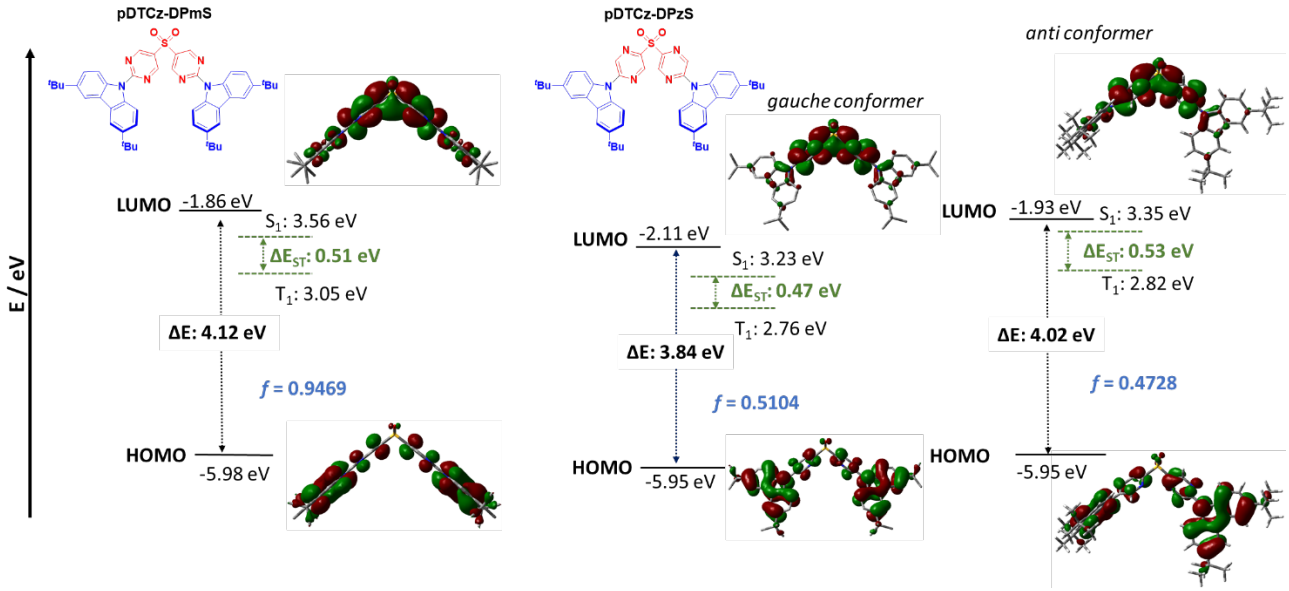

Figure **3**. Calculated HOMO, LUMO, S_1 and T_1 energies, as well as HOMO and LUMO topologies (isovalue = 0.02) of **pDTCz-DPmS** and **pDTCz-DPzS**.

The calculated oscillator strengths, *f*, for the transition to the S_1 state are 0.51 and 0.47 for the *gauche* and *anti* conformers of **pDTCz-DPzS**, respectively, which are quite similar to the corresponding values in **pDTCz-2DPyS** (0.35) and **pDTCz-3DPyS**[13] (0.78). In contrast, *f* reaches 0.94 in **pDTCz-DPmS**, reflecting the much greater overlap between the HOMO and the LUMO in this compound (Figures **3, S10**). For **pDTCz-DPmS** (a similar case to that computed for **pDTCz-3DPyS**), the two pyrimidine nitrogen atoms engage in hydrogen bonding with the hydrogen atoms bound to C-1 and C-8 of the **DTCz**, generating a flattened conformation between the donor and bridge part (0.67°).

Both pyrimidine and pyrazine-based acceptors are of comparable electron-withdrawing strength (Figures **S11-12**); however, coupling them with donors (**TCz**) produces different excited state energies of the emitters. The higher-lying LUMO of the **DPmS** acceptor governs the higher excited state energies of **pDTCz-DPmS** as compared to those of both conformations of **pDTCz-DPzS**. Calculated ΔE_{ST} values for both new emitters (for **pDTCz-DPzS** *gauche* conformer, ΔE_{ST} = 0.47 eV and for *anti* conformer ΔE_{ST} = 0.53 eV, and for **pDTCz-DPmS** ΔE_{ST} = 0.51 eV) are similar to those predicted for the pyridyl sulfone analogues (**pDTCz-2DPyS** and **pDTCz-3DPyS**). Overall, the use of pyrimidine and pyrazine instead of pyridine as bridging units resulted in stabilized HOMO and LUMO levels and S_1 states of **pDTCz-DPmS** and **pDTCz-DPzS**, as compared to the previously reported **pDTCz-2DPyS** and **pDTCz-3DPyS**, with **pDTCz-DPzS** showing the most stabilized LUMO level and S_1 state of the series.

Thermal analysis

The thermal stability of the two emitters was investigated by thermogravimetric analysis (TGA) and differential thermal analysis (DTA). Both compounds exhibited high melting (T_m) and degradation temperatures (T_d). The T_m for **pDTCz-DPmS** and **pDTCz-DPzS** are 399 °C and 392 °C, which are much higher than those of **pDTCz-2DPyS** (353 °C) and **pDTCz-3DPyS** (361 °C) while the T_d (weight loss of 5%) are 416 °C and 446 °C, which are similar to **pDTCz-2DPyS** (391 °C) and **pDTCz-3DPyS** (448 °C) (Figure **S13**). Considering almost the same molecular weight of all four compounds, the observed substantially higher T_m for **pDTCz-DPmS** and **pDTCz-DPzS** can be ascribed in part to the existence of the greater intramolecular hydrogen bonding in these compounds as compared to the pyridine analogues.

Electrochemistry

Electrochemical measurements for **pDTCz-DPmS** and **pDTCz-DPzS** were carried out in dichloromethane (DCM) in order to determine the energies of the frontier energy levels (Figure **4**). The cyclic voltammetry (CV) trace of **pDTCz-DPmS** shows an irreversible reduction wave at E_{pc} = -1.83 V while the CV trace of **pDTCz-DPzS** shows a pseudo-reversible reduction wave with E_{pc} = -1.42 V. The differential pulse voltammetry (DPV) traces of **pDTCz-DPmS** and **pDTCz-DPzS** show reduction peaks at -1.82 V and -1.46 V, respectively. From this, the "LUMO levels" of **pDTCz-DPmS** and **pDTCz-DPzS** can be estimated to be -2.64 eV and -3.00 eV, respectively, from the DPVs. Compared to the corresponding values in **pDTCz-3DPyS** (-2.57 eV) and **pDTCz-2DPyS** (-2.73 eV), one notes a stronger stabilization in **pDTCz-DPzS** whereas **pDTCz-DPmS** shows an intermediate behavior; these results are in line with the LUMO energies calculated by DFT. The oxidation wave for **pDTCz-DPmS** is irreversible and E_{pa} =1.58 V, while the oxidation wave for **pDTCz-DPzS** is pseudo-reversible at E_{pa} = 1.48 V. The DPV traces of **pDTCz-DPmS** and **pDTCz-DPzS** show oxidation peaks at 1.48 V and 1.50 V, respectively. The corresponding levels of **pDTCz-DPmS** and **pDTCz-DPzS** are calculated to be -5.94 eV and -5.96 eV, respectively. The "HOMO values" of **pDTCz-DPmS** and **pDTCz-DPzS** are deeper than those of **pDTCz-3DPyS** (-5.71 eV) and **pDTCz-2DPyS** (-5.71 eV). The oxidation of the emitters was also investigated in neat films by ambient photoelectron spectroscopy (APS). The resulting energies of -5.76 eV were measured for **pDTCz-DPmS** and -5.64 eV for **pDTCz-DPzS** (Figure **S14**) that are somewhat shallower than those found in electrochemistry measurements conducted in DCM, which is not unexpected considering the polarity of the solvent.

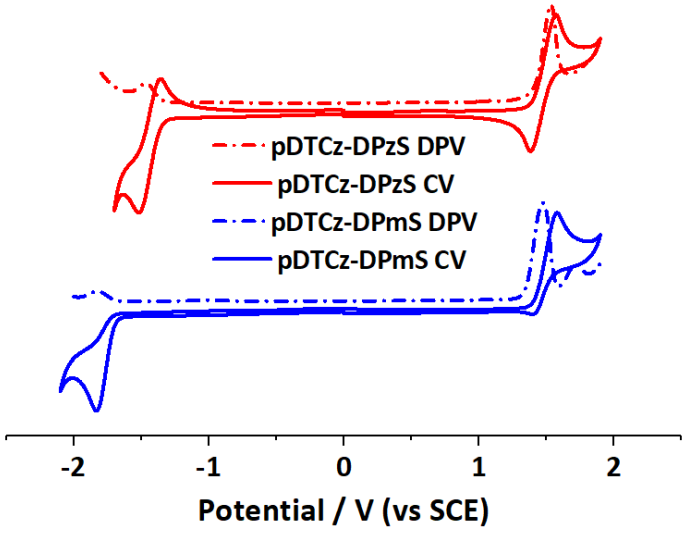

Figure **4**. CVs and DPVs of **pDTCz-DPmS** and **pDTCz-DPzS** in DCM, reported versus SCE (Fc/Fc^+ = 0.34 V in DCM[19], scan rate = 50 mV s^{-1}).

Photophysical Characterization

Figure **5a** shows the UV-visible absorption spectra of **pDTCz-DPmS** and **pDTCz-DPzS** in dimethylformamide (DMF). The presence of an additional nitrogen atom within the heterocycle has a significant impact of the electronic properties compared to the reference pyridylsulfone emitters previously reported.[13] In both **pDTCz-DPmS** and **pDTCz-DPzS** there are pronounced low energy bands at 354 nm and 389 nm, respectively. In line with TD-DFT calculations, these transitions have both π–π* character and significant CT character. While the UV-visible absorption spectrum of **pDTCz-DPmS** resembles that of **pDTCz-3DPyS**, a distinct red-shifted low energy band is apparent in **pDTCz-DPzS** that reflects the stronger electron-acceptor present in **pDTCz-DPzS**. The higher energy bands are at similar energies (280-330 nm) to those of **pDTCz-2DPyS** and **pDTCz-3DPyS**, indicating the donor-localized π-π* transitions (see Figure **S15** for a cross-comparison of the absorption spectra of the four emitters).

Figures **5b** and **5c** show the normalized steady-state photoluminescence (PL) spectra of **pDTCz-DPmS** and **pDTCz-DPzS**, respectively, in dilute toluene, DCM and DMF. In all three solvents, the PL spectra show emission with a CT character, evidenced by their Gaussian band shape and positive solvatochromism. As expected, **pDTCz-DPzS** shows a red-shifted emission compared to that of **pDTCz-DPmS**. Moreover, the magnitude of the positive solvatochromism is larger in **pDTCz-DPzS**, indicating stronger CT occurring in this compound, in line with the frontier orbitals. It is noteworthy that the emission energies in DCM and DMF are nearly the same, implying a saturation of CT stabilization in the relatively low polarity solvent DCM. The phosphorescence (PH) of both emitters was investigated in DCM frozen glass (Figure **S16**). PL collected at 77 K with a time delay longer than 1 ms was assigned as originating from the lowest energy triplet excited state

(T_1). In both emitters, the phosphorescence spectra show some vibrational structure and are essentially unaffected by the medium. Thus, the PH is assigned to have a state with locally excitation (LE) character.

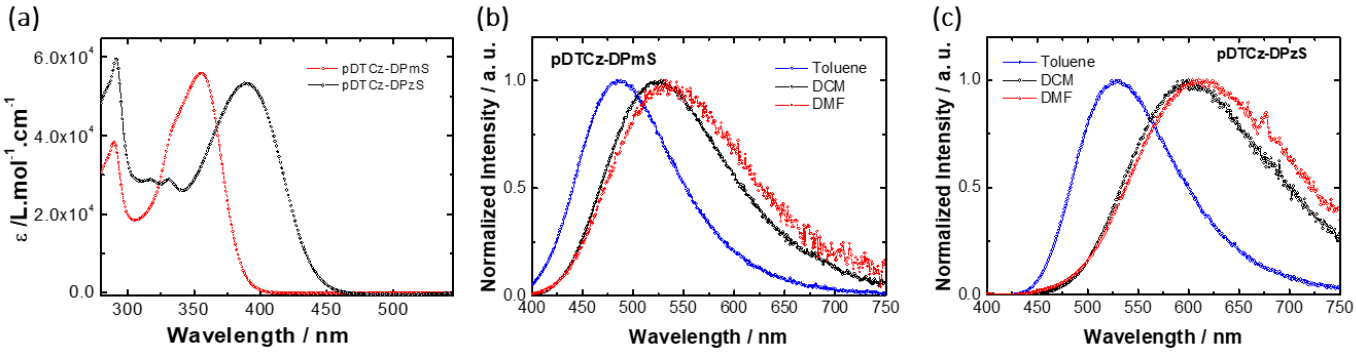

Figure **5**. a) UV-visible absorption spectra of **pDTCz-DPmS** and **pDTCz-DPzS** in DMF. b) Normalized photoluminescence (PL) spectra of **pDTCz-DPmS** and c) **pDTCz-DPzS** in toluene, DCM and DMF. All measurements were performed at room temperature and in air. PL measurements were performed with excitation at 340 nm.

We next investigated the photophysical properties of the two emitters in a range of different matrices with 10 wt% doping in order to determine the most appropriate host material to be used in OLEDs (Figure **6a**). These include: 3,3-di(9H-carbazol-9-yl)-biphenyl (mCBP),[20] *N,N*-9-dicarbazolyl3,5-benzene (mCP),[21] 2,8-bis(diphenylphosphoryl)dibenzo[b,d]thiophene (PPT),[22] and bis[2-(diphenylphosphino)phenyl] ether oxide (DPEPO)[23]. For a comparison, dispersions of emitters in a poly(methylmethacrylate) (PMMA)[24] matrix were also investigated (see Figure **S17**). Emission from CT states is observed in all hosts; for **pDTCz-DPmS**, there is very little sensitivity to the polarity of the host while for **pDTCz-DPzS** a more pronounced bathochromic shift is observed with increasing host polarity (e.g., DPEPO and PPT). This is in line with the solution-state behaviour (Figures **5b** and **5c**) and reflects the greater CT character of the latter emitter.

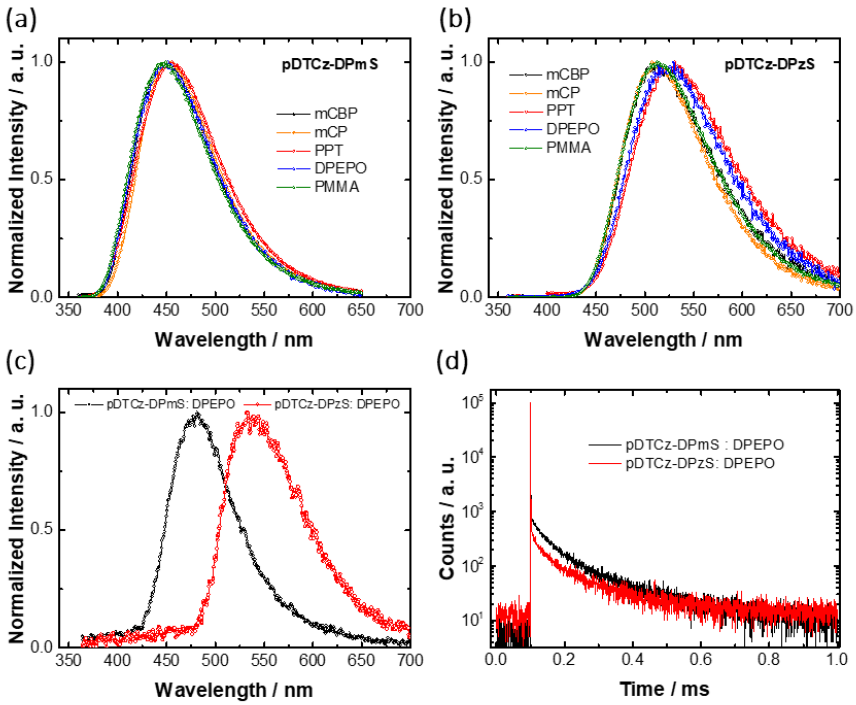

Figure **6**. a) Normalized PL spectra of 10 wt% **pDTCz-DPmS** and b) 10 wt% **pDTCz-DPzS** in different host materials (mCBP, mCP, PPT, DPEPO and PMMA) at room temperature with excitation at 340 nm. c) Phosphorescence spectra of 10 wt% **pDTCz-DPmS:**DPEPO and **pDTCz-DPzS**:DPEPO at 77 K with excitation at 343 nm. d) Time-resolved PL decay traces of 10 wt%. **pDTCz-DPmS**:DPEPO and **pDTCz-DPzS**:DPEPO with wavelength of collection at 470 nm and 520 nm, respectively, at room temperature with excitation at 379 nm and under vacuum.

DPEPO was chosen to be the most appropriate host for both emitters due to its high triplet energy, suitable HOMO-LUMO levels and high Φ_{PL} values for **pDTCz-DPmS** and **pDTCz-DPzS** observed in this host. The Φ_{PL} under a nitrogen flow was measured to be 73% for **pDTCz-DPmS**:DPEPO and 68% for **pDTCz-DPzS**:DPEPO films and these values decreased to 63% and 59% under air. Both emitters were expected to show similar Φ_{PL} as they show equivalent extinction coefficient values in their absorption spectra (see Figure **5a**). These values are similar to our reference compounds, **pDTCz-2DPyS:**DPEPO (81%) and **pDTCz-3DPyS:**DPEPO (72%)**,** and reflect the supressed non-radiative decay in these emitters.

The T_1 energies were determined from the onset of the phosphorescence spectra in DPEPO host and are 2.92 eV and 2.56 eV for **pDTCz-DPmS** and **pDTCz-DPzS**, respectively (Figure **6c**). Singlet energies, estimated from the onset of PL spectra at room temperature in DPEPO host, are 3.07 eV and 2.72 eV for the **pDTCz-DPmS** and **pDTCz-DPzS**, respectively. Both emitters therefore possess small ΔE_{ST} values of 150 and 160 meV for **pDTCz-DPmS** and **pDTCz-DPzS**, respectively, indicating a very low energy barrier for rISC to occur. Both

pDTCz-DPmS and **pDTCz-DPzS** possess lower ΔE_{ST} values than **pDTCz-2DPyS** (220 meV) and **pDTCz-3DPyS** (210 meV) measured also in DPEPO films, confirming the enhancement of TADF by use of pyrimidine and pyrazine over pyridine-based analogues. Figure **S18** shows the energy level diagram of the experimentally determined S_1 and T_1 states of all four emitters, highlighting that the addition of N atoms in the bridging units strongly modulates the S_1 and T_1 energies. When comparing **pDTCz-DPmS** and **pDTCz-3DPyS**, it is clear that the S_1 state, which has a dominant CT character, is intensely affected by changes in the D-A conformation, while the conformation affects less the T_1 energies, which show LE character, resulting in a reduced ΔE_{ST}. We note that the measured ΔE_{ST} values are significantly smaller than their DFT counterparts, which is the usual trends for organic molecules, as proven by calculations performed on Thiel's sets.[25]

Figure **6d** shows the emission decay curves of **pDTCz-DPmS**:DPEPO and **pDTCz-DPzS**:DPEPO films measured under vacuum at room temperature. Both films show delayed fluorescence with average lifetime, $\tau_{DF,}$ of 127 μs and 108 μs, respectively. TADF was identified to be the main mechanism responsible to generate the DF in both emitters as the magnitude of the delayed fluorescence was found to be temperature dependent (Figure **S19**). These values are much smaller than those found in **pDTCz-2DPyS** (τ_d = 809 μs) and **pDTCz-3DPyS** (τ_d = 288 μs) measured also in DPEPO films.[13] The decreased values found in our current emitters is a consequence of faster rISC due to the smaller ΔE_{ST} values and this feature leads to improved efficiency roll-off as discussed in the device section. The prompt fluorescence, τ_p, lifetimes of **pDTCz-DPmS** and **pDTCz-DPzS** were also investigated at room temperature using a short time window (100 ns) and found to have average lifetime of 6 ns and 10 ns, respectively (Figure **S20**). The PF and DF decays for both emitters are complex, requiring bi-exponential fits to both the prompt and the delayed components (Figure **S21**). The interpretation of such fluorescence decays is not straightforward and such behaviour has been observed in many other TADF emitters, including the pyridine-based analogues (**pDTCz-3DPyS** and **pDTCz-2DPyS**). Multi-exponential decay indicates heterogeneity in the sample and this could arise from distinct molecular conformations that the emitters can adopt in the solid state. Conformations with larger energy gap between the singlet and triplet states, would have slower DF components and consequently slower rISC rates.[26–29] The photophysical properties in the solid state of both emitters are summarized in Table **1**.

Table **1.** Photophysical properties of **pDTCz-DPmS**, **pDTCz-DPzS**, **pDTCz-3DPyS**,[13] and **pDTCz-2DPyS**,[13] in DPEPO host.

	S_1 / eV	T_1 / eV	ΔE_{ST} / eV	Φ_{PL} / %	τ_{PF} / ns	τ_{DF} / µs
pDTCz-DPmS	3.07	2.92	0.15	73	6	127
pDTCz-DPzS	2.72	2.56	0.16	68	10	108
pDTCz-3DPyS	3.16	2.95	0.21	72	7	288
pDTCz-2DPyS	3.06	2.84	0.22	81	13	809

S_1= singlet state energy obtained from the onset of the photoluminescence spectra measured at room temperature with excitation wavelength at 340 nm; T_1 = triplet state energy obtained from the onset of the phosphorescence spectra measured at 77 K with excitation wavelength at 343 nm; $\Delta E_{ST} = E(S_1) - E(T_1)$; Φ_{PL} = photoluminescence quantum yield measured using an integrating sphere under nitrogen flow with excitation wavelength at 300 nm; τ_{PF} = average prompt fluorescence lifetime measured at room temperature with time window of 100 ns. τ_{DF} = average delayed fluorescence lifetime measured at room temperature with time window of 1 ms; All measurements were performed in co-doped DPEPO film (10 wt%).

Device Performance

We next fabricated vacuum-sublimed OLEDs. The architecture of the devices was: ITO/TAPC (40nm)/mCP (10nm)/10 wt% emitter:DPEPO (30nm)/DPEPO (10nm)/TmPyPB (40nm)/LiF (1nm)/Al (100nm). ITO is indium tin oxide, TAPC is 4,4′-cyclohexylidenebis[*N,N*-bis(4-methylphenyl)benzenamine], TmPyPB is 1,3,5-tri(*m*-pyridin-3-ylphenyl)benzene (Figure **7a**). Table **2** highlights the relevant OLED metrics for the representative devices tested (Figure **S22**). Figure **7b** shows the electroluminescence (EL) spectra of **pDTCz-DPmS**:DPEPO (D1) and **pDTCz-DPzS**:DPEPO (D2) devices. The CIE chromaticity coordinates are (0.19, 0.26) and (0.31, 0.53) for D1 and D2. Device D1 shows blue EL spectra while device D2 is green, which is consistent with the stronger acceptor used in **pDTCz-DPzS** emitter.

Figure **7c** shows a representative EQE versus brightness curve for both devices. Device D1 shows an EQE_{max} of 14% at 6 cd/m^2. The EQE values of device D1 decrease considerably at 100 cd/m^2 (EQE_{100} = 7%), which is likely due to poor charge balance in the device owing to the n-type nature of the DPEPO host. The device shows a low turn-on voltage (~ 3.5 eV) and brightness levels reaching 240 cd/m^2 (EQE = 2.9%). Device D2 shows an EQE_{max} of 18% at 15 cd/m^2. At 100 cd/m^2, the EQE value is still high at EQE_{100} of 14%. Device D2 also shows a low turn-on voltage (~ 4.3 eV) and brightness levels reaching higher levels, 961 cd/m^2 (EQE = 4.1%). See Figure **S23** for J×V curves.

Given the high Φ_{PL} of 73% and 68% in DPEPO for **pDTCz-DPmS** and **pDTCz-DPzS**, respectively, and considering charge balance as 100%, outcoupling efficiency ~ 25-30%,[30] and also considering that 100% of the triplet excitons are being harvested and converted to singlet excitons via the TADF mechanism, the theoretical

EQE_{max} for **pDTCz-DPmS** and **pDTCz-DPzS** are ~18-22% and ~17-20%, respectively. Thus, the theoretical and experimental EQE_{max} values of **pDTCz-DPzS**-based devices align. However, the **pDTCz-DPmS**-based devices show lower EQE values than expected theoretically, which is likely related to the triplet energy of the host and the mCP hole-transporting layer (HTL). Since the triplet energy of DPEPO is close in energy to that of **pDTCz-DPmS** it is likely that it will serve as a quencher in the D1 devices. In addition, mCP has an even lower triplet energy than **pDTCz-DPmS** and so we can also expect quenching of triplet excitons at the HTL-EML interface in these devices.

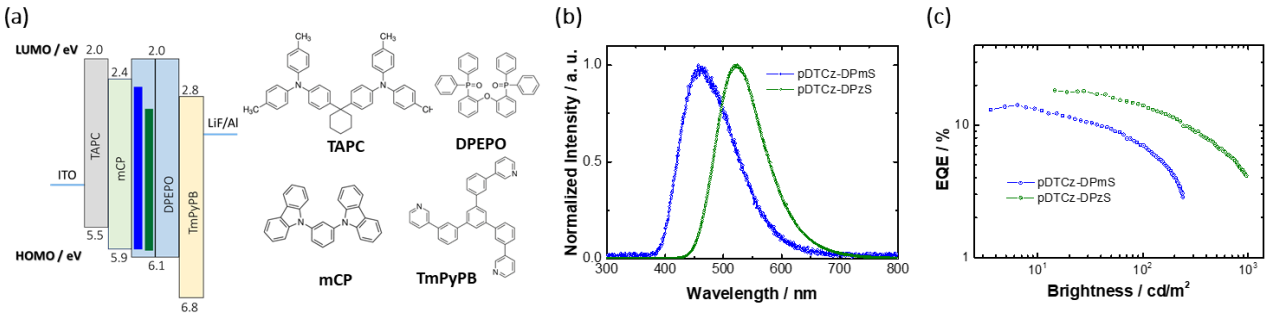

Figure **7**. a) Device architecture and molecular structures of materials used in **pDTCz-DPmS**:DPEPO (D1) and **pDTCz-DPmS**:DPEPO (D2) devices. Blue bar represents the HOMO-LUMO of **pDTCz-DPmS** and green bar that of **pDTCz-DPzS** b) Electroluminescence (EL) spectrum c) external quantum efficiencies versus brightness curves of D1 and D2 devices.

Compared to our previously reported OLEDs with **pDTCz-3DPyS** and **pDTCz-2DPyS** as the emitters dispersed in DPEPO, the present devices show improvements in both EQE_{max} and EQE_{100} values. The EQE_{max} increased from 13% **pDTCz-3DPyS**:DPEPO and 11% **pDTCz-2DPyS:**DPEPO to 14% in **pDTCz-DPmS**:DPEPO and 18% in **pDTCz-DPzS**:DPEPO. However, the greatest improvement in device performance is related to the efficiency roll-off. The **pDTCz-3DPyS**:DPEPO OLED showed a drop of 66% from its EQE_{max} value at 100 cd/m^2 while for the **pDTCz-2DPyS**:DPEPO OLED the efficiency roll-off is 63%. The present devices, however, show smaller efficiency roll-offs of 50% and 22% for devices D1 and D2, respectively. We hypothesize that the intramolecular hydrogen bonding within the investigated emitters contribute both to improvements in the EQE_{max} and efficiency roll-off as compared to our previously reported pyridine analogues, observations in line with those found in the literature.[31,32] On the other hand, the **pDTCz-3DPyS**:DPEPO and **pDTCz-2DPyS**:DPEPO devices show sharp blue EL spectra. While device D1 shows a slightly red-shifted λ_{EL} of 461 nm compared to **pDTCz-3DPyS**:DPEPO (λ_{EL} = 452 nm) and a similar EL maximum to **pDTCz-2DPyS**:DPEPO (λ_{EL} = 466 nm), its spectrum is broader, reflected by the larger full width at half maximum (FWHM). For device D2 the λ_{EL} of 521 nm is strongly red-shifted. Therefore, with the addition of a second nitrogen atom in the bridge of the emitters there is significant improvement in device performance, but at the cost of lower color purity.

Table **2.** Electrical properties of **OLEDs** with **pDTCz-DPmS** and **pDTCz-DPzS** as the emitters.[a]

Device	V_{on} / V	EQE_{max} / %	EQE_{100} / %	Lum_{max}/cd/m^2	CIE (x,y)	λ_{EL} / nm
D1: pDTCz-DPmS: DPEPO	~3.6	14	7	240	(0.19, 0.26)	461
D2: pDTCz-DPzS: DPEPO	~ 4.4	18	14	961	(0.31, 0.53)	522

[a.] V_{on} = Turn on voltage; EQE = External quantum efficiency; Lum = luminance. Subscripts 100 refer to values taken at 100 cd/m^2. CIE = Internationale de L'Éclairage coordinates and EL = electroluminescence.

Conclusions

We have designed two isomeric D-A-D emitters 9,9'-(sulfonylbis(pyrimidine-5,2-diyl))bis(3,6-di-*tert*-butyl-9H-carbazole) (**pDTCz-DPmS**) and 9,9'-(sulfonylbis(pyrazine-5,2-diyl))bis(3,6-di-*tert*-butyl-9H-carbazole) (**pDTCz-DPzS**) with acceptor moieties containing pyrimidine and pyrazine groups. Both emitters show strong charge transfer transitions to the lowest singlet states and small energy gaps between the excited singlet and triplet states (ΔE_{ST} < 160 meV), which lead to occurrence of delayed fluorescence via a TADF mechanism. Both emitters showed high photoluminescence quantum yields of between 68-73% when dispersed in DPEPO host. Vacuum-deposited OLEDs demonstrated blue and green electroluminescence spectra with EQE_{max} of 14% (at 6 cd/m^2) and 18% (at 15 cd/m^2) using **pDTCz-DPmS** and **pDTCz-DPzS** as emitters, respectively. These OLEDs showed improved EQE values and efficiency roll-off when compared to the devices using reference emitters: **pDTCz-3DPyS** (EQE_{max} = 13% at 1.4 cd/m^2) and **pDTCz-2DPyS** (EQE_{max} = 11% at 4.5 cd/m^2). These improvements result from the more planar donor-bridge conformations that are stabilized by intramolecular hydrogen bonding adopted by both **pDTCz-DPmS** and **pDTCz-DPzS**. These results show that small changes in the structure of the bridge unit play a crucial role in achieving highly efficient TADF OLEDs. However, these device improvements come at a cost of color purity, as the electroluminescence spectra of both **pDTCz-DPmS** and **pDTCz-DPzS** are red-shifted and broader when compared to those of devices with the reference emitters.

Experimental

Electrochemistry measurements

Cyclic Voltammetry (CV) analysis was performed on an Electrochemical Analyzer potentiostat model 620E from CH Instruments at a sweep rate of 100 mV/s. Differential pulse voltammetry (DPV) was conducted with an increment potential of 0.004 V and a pulse amplitude, width, and period of 50 mV, 0.05, and 0.5 s,

respectively. Samples were prepared as dichloromethane (DCM) solutions, which were degassed by sparging with DCM-saturated nitrogen gas for 15 minutes prior to measurements. All measurements were performed using 0.1 M DCM solution of tetra-n-butylammonium hexafluorophosphate ([nBu$_4$N]PF$_6$]). An Ag/Ag$^+$ electrode was used as the reference electrode while a platinum electrode and a platinum wire were used as the working electrode and counter electrode, respectively. The redox potentials are reported relative to a saturated calomel electrode (SCE) with a ferrocenium/ferrocene (Fc/Fc$^+$) redox couple as the internal standard (0.34 V vs SCE).[33]

Photophysical measurements

Three types of samples were studied in this work: i) solution, ii) spin-coated films and iii) evaporated films. i) Optically dilute solutions of concentrations on the order of 10^{-5} or 10^{-6} M were prepared in HPLC grade toluene, *N,N*-dimethylformamide (DMF) and DCM; ii) Spin-coated films were produced from chloroform solutions of blends (10 wt% guest to host) at 2000 rpm for 60 seconds; iii) Evaporated films (10% wt) were thermally evaporated onto quartz substrates using an Angstrom deposition chamber at 10^{-7} mbar with final thickness ~ 150 nm. Absorption spectra of solutions were recorded at room temperature on a Shimadzu UV-1800 double beam spectrophotometer with a 1 cm quartz cuvette. Molar absorptivity values were determined from at least five independent solutions at varying concentrations with absorbance ranging from 1.16×10^{-5} to 8.69×10^{-6} M. Steady-state emission spectra and time-resolved decay curves were recorded for solutions and spin coating films using an Edinburgh Instruments F980 spectrofluorimeter. The steady-state spectra were recorded at room temperature using excitation at 340 nm (Xenon lamp) while the time-resolved decay curves were recorded at several temperatures (77 K, 200 K, 250 K and 300 K) with excitation at 378 nm (PDL 800-D pulsed diode laser). Time-resolved decay curves for prompt fluorescence (100 ns time window) were recorded using time correlated single photon counting (TCSPC) while time-resolved decay curves for delayed fluorescence (1 ms time window) were recorded using multi-channel scaling (MCS). Time-resolved spectra (phosphorescence) were obtained on evaporated films using a gated intensified charge coupled device (iCCD camera) from Stanford Computer Optics at 77 K and under laser excitation at 343 nm (100 Hz). Photoluminescence quantum yield, Φ_{PL}, measurements were performed on evaporated films using an integrating sphere in a Hamamatsu C9920-02 system[34] with excitation at 300 nm under air and under constant nitrogen gas flow. The error on the Φ_{PL} values are ±5%.

Device fabrication and testing

OLEDs were fabricated using pre-cleaned indium-tin-oxide (ITO) coated glass substrates with ITO thickness of 90 nm. The OLEDs have a pixel area of 2 mm^2. The small molecule and cathode layers were thermally evaporated using an Angstrom deposition chamber at 10^{-7} mbar at 0.3 A/s or 0.6 A/s for organic layers and 1 A/s for the cathode. OLED testing was performed using a sourcemeter (Keithey 2400) and photodiode, and data analysed assuming Lambertian emission. Eletroluminescence spectra were collected using a spectrograph (MS125, Oriel) coupled to a CCD camera (DV420-BU, Andor).

Acknowledgements

We are grateful to the Engineering and Physical Sciences Research Council (EPSRC) for support from grants EP/P010482/1 and EP/R035164/1. P. Rajamalli acknowledges support from a Marie Skłodowska-Curie Individual Fellowship (MCIF; No. 749557). Dongyang Chen thanks the China Scholarship Council (grant numbers 201603780001). This work used the computational resources of the CCIPL centre installed in Nantes thanks to the support of the *Région des Pays de la Loire*.

Supporting Information

Instrumentation details, synthesis and chemical characterization (NMR spectra, elemental analysis reports, HPLC chromatograms), crystal structure information (CCDC: 1951421-1951423), computational details, theoretical electron acceptor analysis, ambient pressure air photoemission spectra, photophysical and thermal properties as well as device characterization are available in supporting information.

References

(1) Brown, A. R.; Pichler, K.; Greenham, N. C.; Bradley, D. D. C.; Friend, R. H.; Holmes, A. B. Optical Spectroscopy of Triplet Excitons and Charged Excitations in Poly(p-Phenylenevinylene) Light-Emitting Diodes. *Chem. Phys. Lett.* **1993**, *210* (1–3), 61–66.

(2) Uoyama, H.; Goushi, K.; Shizu, K.; Nomura, H.; Adachi, C. Highly Efficient Organic Light-Emitting Diodes from Delayed Fluorescence. *Nature* **2012**, *492* (7428), 234–238.

(3) dos Santos, P. L.; Etherington, M. K.; Monkman, A. P. Chemical and Conformational Control of the Energy Gaps Involved in the Thermally Activated Delayed Fluorescence Mechanism. *J. Mater. Chem. C* **2018**, *6* (18), 4842–4853.

(4) Bui, T.-T.; Goubard, F.; Ibrahim-Ouali, M.; Gigmes, D.; Dumur, F. Recent Advances on Organic Blue Thermally Activated Delayed Fluorescence (TADF) Emitters for Organic Light-Emitting Diodes (OLEDs). *Beilstein J. Org. Chem.* **2018**, *14*, 282–308.

(5) Wong, M. Y.; Krotkus, S.; Copley, G.; Li, W.; Murawski, C.; Hall, D.; Hedley, G. J.; Jaricot, M.; Cordes, D. B.; Slawin, A. M. Z.; Olivier, Y.; Beljonne, D.; Muccioli, L.; Moral, M.; Sancho-Garcia, J.; Gather, M. C.; Samuel, I. D. W.; Zysman-Colman, E. Deep-Blue Oxadiazole-Containing Thermally Activated Delayed Fluorescence Emitters for Organic Light-Emitting Diodes. *ACS Appl. Mater. Interfaces* **2018**, *10* (39), 33360–33372.

(6) Ahn, D. H.; Kim, S. W.; Lee, H.; Ko, I. J.; Karthik, D.; Lee, J. Y.; Kwon, J. H. Highly Efficient Blue Thermally Activated Delayed Fluorescence Emitters Based on Symmetrical and Rigid Oxygen-

Bridged Boron Acceptors. *Nat. Photonics* **2019**, *13* (8), 540–546.

(7) Stachelek, P.; Ward, J. S.; dos Santos, P. L.; Danos, A.; Colella, M.; Haase, N.; Raynes, S. J.; Batsanov, A. S.; Bryce, M. R.; Monkman, A. P. Molecular Design Strategies for Color Tuning of Blue TADF Emitters. *ACS Appl. Mater. Interfaces* **2019**, *11* (30), 27125–27133.

(8) Zhang, X.; Fuentes-Hernandez, C.; Zhang, Y.; Cooper, M. W.; Barlow, S.; Marder, S. R.; Kippelen, B. High Performance Blue-Emitting Organic Light-Emitting Diodes from Thermally Activated Delayed Fluorescence: A Guest/Host Ratio Study. *J. Appl. Phys.* **2018**, *124* (5), 055501.

(9) Gibson, J.; Monkman, A.; Penfold, T. The Importance of Vibronic Coupling for Efficient Reverse Intersystem Crossing. *ChemPhysChem* **2016**, *17*, 2956–2961.

(10) Santos, P. L.; Ward, J. S.; Data, P.; Batsanov, A. S.; Bryce, M. R.; Dias, F. B.; Monkman, A. P. Engineering the Singlet–Triplet Energy Splitting in a TADF Molecule. *J. Mater. Chem. C* **2016**, *4* (17), 3815–3824.

(11) Ward, J. S.; Nobuyasu, R. S.; Batsanov, A. S.; Data, P.; Monkman, A. P.; Dias, F. B.; Bryce, M. R. The Interplay of Thermally Activated Delayed Fluorescence (TADF) and Room Temperature Organic Phosphorescence in Sterically-Constrained Donor–Acceptor Charge-Transfer Molecules. *Chem. Commun.* **2016**, *52* (12), 2612–2615.

(12) Komatsu, R.; Ohsawa, T.; Sasabe, H.; Nakao, K.; Hayasaka, Y.; Kido, J. Manipulating the Electronic Excited State Energies of Pyrimidine-Based Thermally Activated Delayed Fluorescence Emitters To Realize Efficient Deep-Blue Emission. *ACS Appl. Mater. Interfaces* **2017**, *9* (5), 4742–4749.

(13) Rajamalli, P.; Chen, D.; Li, W.; Samuel, I. D. W.; Cordes, D. B.; Slawin, A. M. Z.; Zysman-Colman, E. Enhanced Thermally Activated Delayed Fluorescence through Bridge Modification in Sulfone-Based Emitters Employed in Deep Blue Organic Light-Emitting Diodes. *J. Mater. Chem. C* **2019**, *7* (22), 6664–6671.

(14) Zhang, Q.; Li, J.; Shizu, K.; Huang, S.; Hirata, S.; Adachi, C.; Adachi, P. C.; Zhang, Q.; Li, J.; Shizu, K.; Hirata, S.; Miyazaki, H. Design of Efficient Thermally Activated Delayed Fluorescence Materials for Pure Blue Organic Light Emitting Diodes. *J. Am. Chem. Soc.* **2012**, *134* (36), 14706–14709.

(15) Pople, J. A.; Binkley, J. S.; Seeger, R. Theoretical Models Incorporating Electron Correlation. *Int. J. Quantum Chem.* **2009**, *10* (S10), 1–19.

(16) Perdew, J. P.; Ernzerhof, M.; Burke, K. Rationale for Mixing Exact Exchange with Density Functional Approximations. *J. Chem. Phys.* **1996**, *105* (22), 9982–9985.

(17) Grimme, S. Density Functional Calculations with Configuration Interaction for the Excited States of Molecules. *Chem. Phys. Lett.* **1996**, *259* (1–2), 128–137.

(18) Hirata, S.; Head-Gordon, M. Time-Dependent Density Functional Theory within the Tamm–Dancoff Approximation. *Chem. Phys. Lett.* **1999**, *314* (3–4), 291–299.

(19) Gritzner, G.; Kuta, J. Recommendations on Reporting Electrode Potentials in Nonaqueous Solvents *Pure Appl. Chem.* **1984**, *56* (4), 461–466.

(20) Oh, C. S.; Lee, J. Y.; Noh, C. H.; Kim, S. H. Molecular Design of Host Materials for High Power

Efficiency in Blue Phosphorescent Organic Light-Emitting Diodes Doped with an Imidazole Ligand Based Triplet Emitter. *J. Mater. Chem. C* **2016**, *4* (17), 3792–3797.

(21) Kim, J. W.; You, S. Il; Kim, N. H.; Yoon, J.-A.; Cheah, K. W.; Zhu, F. R.; Kim, W. Y. Study of Sequential Dexter Energy Transfer in High Efficient Phosphorescent White Organic Light-Emitting Diodes with Single Emissive Layer. *Sci. Rep.* **2015**, *4* (1), 7009.

(22) Jeong, S. H.; Lee, J. Y. Dibenzothiophene Derivatives as Host Materials for High Efficiency in Deep Blue Phosphorescent Organic Light Emitting Diodes. *J. Mater. Chem.* **2011**, *21* (38), 14604.

(23) Zhang, J.; Ding, D.; Wei, Y.; Xu, H. Extremely Condensing Triplet States of DPEPO-Type Hosts through Constitutional Isomerization for High-Efficiency Deep-Blue Thermally Activated Delayed Fluorescence Diodes. *Chem. Sci.* **2016**, *7* (4), 2870–2882.

(24) Ali, U.; Karim, K. J. B. A.; Buang, N. A. A Review of the Properties and Applications of Poly (Methyl Methacrylate) (PMMA). *Polym. Rev.* **2015**, *55* (4), 678–705.

(25) Jacquemin, D.; Duchemin, I.; Blondel, A.; Blase, X. Benchmark of Bethe-Salpeter for Triplet Excited-States. *J. Chem. Theory Comput.* **2017**, *13* (2), 767–783.

(26) Zhang, Q.; Kuwabara, H.; Potscavage, W. J.; Huang, S.; Hatae, Y.; Shibata, T.; Adachi, C. Anthraquinone-Based Intramolecular Charge-Transfer Compounds: Computational Molecular Design, Thermally Activated Delayed Fluorescence, and Highly Efficient Red Electroluminescence. *J. Am. Chem. Soc.* **2014**, *136* (52), 18070–18081.

(27) dos Santos, P. L.; Ward, J. S.; Congrave, D. G.; Batsanov, A. S.; Eng, J.; Stacey, J. E.; Penfold, T. J.; Monkman, A. P.; Bryce, M. R. Triazatruxene: A Rigid Central Donor Unit for a D-A 3 Thermally Activated Delayed Fluorescence Material Exhibiting Sub-Microsecond Reverse Intersystem Crossing and Unity Quantum Yield via Multiple Singlet-Triplet State Pairs. *Adv. Sci.* **2018**, *5* (6), 1700989.

(28) Northey, T.; Stacey, J.; Penfold, T. J. The Role of Solid State Solvation on the Charge Transfer State of a Thermally Activated Delayed Fluorescence Emitter. *J. Mater. Chem. C* **2017**, *5* (42), 11001–11009.

(29) Nobuyasu, R. S.; Ward, J. S.; Gibson, J.; Laidlaw, B. A.; Ren, Z.; Data, P.; Batsanov, A. S.; Penfold, T. J.; Bryce, M. R.; Dias, F. B. The Influence of Molecular Geometry on the Efficiency of Thermally Activated Delayed Fluorescence. *J. Mater. Chem. C* **2019**, *7* (22), 6672–6684.

(30) Gather, M. C.; Reineke, S. Recent Advances in Light Outcoupling from White Organic Light-Emitting Diodes. *J. Photon. Energy* **2015**, *5* (1), 057607.

(31) Pandidurai, J.; Jayakumar, J.; Senthilkumar, N.; Cheng, C.-H. Effects of Intramolecular Hydrogen Bonding on the Conformation and Luminescence Properties of Dibenzoylpyridine-Based Thermally Activated Delayed Fluorescence Materials. *J. Mater. Chem. C* **2019**, *7* (42), 13104–13110.

(32) Ma, F.; Cheng, Y.; Zhang, X.; Gu, X.; Zheng, Y.; Hasrat, K.; Qi, Z. Enhancing Performance for Blue TADF Emitters by Introducing Intramolecular CH···N Hydrogen Bonding between Donor and Acceptor. *Dye. Pigment.* **2019**, *166*, 245–253.

(33) Connelly, N. G.; Geiger, W. E. Chemical Redox Agents for Organometallic Chemistry. *Chem. Rev.*

1996, *96* (2), 877–910.

(34) Greenham, N. C.; Samuel, I. D. W.; Hayes, G. R.; Phillips, R. T.; Kessener, Y. A. R. R.; Moratti, S. C.; Holmes, A. B.; Friend, R. H. Measurement of Absolute Photoluminescence Quantum Efficiencies in Conjugated Polymers. *Chem. Phys. Lett.* **1995**, *241* (1–2), 89–96.

TOC Graphic